ANALYTICAL SCIENCES DECEMBER 2020, VOL. 36

A Heterocyclic-based Bifunctional Sensor for Detecting Cobalt and Zinc Ion

Haeri So, Hangyul Lee, and Cheal Kim†

Department of Fine Chemistry, Seoul National University of Science and Technology, Seoul 01178, Korea

A new bifunctional chemosensor **HBP** ((*E*)-2-(2-((5-bromopyridin-2-yl)methylene)hydrazinyl) quinoline) based on heterocyclic compounds was designed and studied. The **HBP** showed successful detecting ability toward cobalt ion with a UV-visible red-shift and a color change of colorless to pink. Moreover, toward zinc ion, the **HBP** showed an obvious fluorescence turn-on response. The binding ratio of the **HBP** to cobalt and zinc was a 2 to 1 for both ions. The detection limits were found to be 10 nM for Co^{2+} and 18 nM for Zn^{2+}. Based on UV-vis and fluorescent spectral variations, Job plots, ESI-MS, FT-IR and calculations, the binding mechanisms of the **HBP** toward cobalt and zinc ions were proposed.

Keywords Heterocyclic compound, colorimetric and fluorometric analysis, cobalt ion, zinc ion, calculations

(Received June 6, 2020 Accepted August 18, 2020; Advance Publication Released Online by J-STAGE August 28, 2020)

Introduction

The development of chemosensors for detecting a variety of metal ions has attracted great attention owing to their versatile applicability in pathological, biological, and industrial environments.[1-3] Among various analytical methods, colorimetric and fluorescent assays are strongly preferred as optical methods, because they offer versatile advantages like fast response, and high selectivity and sensitivity.[4-8] Therefore, a wide range of colorimetric and fluorescent sensors have been reported for detecting diverse metal ions.

Among a variety of metal ions, cobalt ion is a crucial micronutrient for plants and animals and participates in the production of vitamin B_{12} as well as other biological products. Zinc ion is well known as the second most plentiful transition metal ion in the body. It is an important component in physiological processes like gene expression, DNA organization, and enzymatic reactions.[9-13] However, a disruption in the concentration level of these metal ions can adversely affect the human body and lead to neurogenic diseases, like Menkes' and Alzheimer's diseases.[14-16] Therefore, it is of great significance to developing chemosensors for detecting cobalt and zinc ions with low detection limits.

Up to now, a large number of chemosensors for cobalt or zinc ion have been reported.[17-24] However, chemosensors capable of detecting both cobalt and zinc ions are very rare,[25-28] though multifunctional chemosensors have attracted much attention because of their advantages, such as higher efficiency and applicability, low cost and easy sample preparation.[29,30] In addition. although a few sensors show selective sensing abilities to cobalt and zinc ions, none of them have a nano molar-level detection limit for both ions. For these reasons, there is still a need to develop chemosensors with nano molar-level detection limits for detecting both ions. Since cobalt and zinc ions prefer to bind to the N donor atom, we envisioned that a chemosensor having a nitrogen-rich environment might selectively sense the two metal ions.

Heterocyclic compounds like quinoline, pyridine and imidazole have a strong ability to bind to metal ions like cobalt and zinc ions because they contain electron-rich atoms, such as nitrogen.[31-34] In particular, a quinoline moiety is a well-known fluorophore as well as a chromophore and is very interesting because it can induce the unique optical response to particular metal ions like Zn^{2+}.[35,36] Moreover, a pyridine moiety containing the electron-withdrawing atom bromine can induce outstanding optical changes with charge transfer.[37,38] Therefore, we expected a chemosensor based on quinoline and pyridine moieties could be a bifunctional detector for metal ions like cobalt and zinc ions through the optical response.

Hence, we developed a heterocyclic-based bifunctional chemosensor, **HBP**, for detecting cobalt and zinc ions. The **HBP** chemosensor showed outstanding optical responses to cobalt and zinc ions, with colorimetry and fluorometry. The proposed binding mechanisms toward cobalt and zinc ions were explained by various spectroscopic techniques, ESI-mass and DFT calculations.

Experimental

Materials and equipment

All chemical reagents were commercially obtained. ^{1}H and ^{13}C NMR data were recorded on a Varian spectrometer. Absorption and fluorescence spectra were recorded by using a Perkin Elmer spectrometer (Lambda 25 UV-Vis and LS45). ESI-MS spectra were collected on a Thermo Finnigan ion trap machine.

† To whom correspondence should be addressed.
E-mail: chealkim@snut.ac.kr

*Procedure for synthesizing **HBP** ((E)-2-(2-((5-bromopyridin-2-yl)methylene)hydrazinyl) quinoline)*

2-Hydrazinylquinoline (0.5 mmol) and 5-bromo-2-pyridinecarboxaldehyde (0.7 mmol) were dissolved in 5 mL of EtOH. With stirring for 3 h, an ivory-colored powder was produced, filtered, and then washed with hexane. Yield: 54%. ^{1}H NMR (DMSO-d_6): 11.74 (s, 1H), 8.68 (s, 1H), 8.24 (d, J = 8.7 Hz, 1H), 8.09 (s, 1H), 8.05 (m, 1H), 8.00 (m, 1H), 7.82 (d, J = 8 Hz, 1H), 7.70 (m, 3H), 7.33 (m, 1H). ^{13}C NMR (DMSO-d_6): 155.3 (1C), 152.9 (1C), 149.9 (1C), 146.9 (1C), 139.2 (1C), 138.7 (1C), 138.2 (1C), 129.8 (1C), 127.9 (1C), 126.0 (1C), 124.4 (1C), 123.0 (1C), 120.6 (1C), 119.1 (1C), 109.4 (1C). ESI-MS: m/z calcd for [**HBP** + H$^+$]$^+$, 327.02; found, 327.33. Element analysis calcd (%) for $C_{15}H_{11}BrN_4$ + 0.5 H_2O: C, 53.59; H, 3.60; N, 16.6 %; found (%): C, 53.48; H, 3.21; N, 16.59%.

Fluorescence and UV-visible studies

For cobalt(II) ion, all UV-visible studies were achieved in bis-tris buffer (10 mM, pH 7.0). A **HBP** stock was made in DMSO at 5 mM concentration and the concentration of **HBP** in all experiments was set as 2 μM. All metal ion stocks containing MNO_3 (M = Na and K) or $M(NO_3)_2$ (M = Zn, Co, Cd, Cu, Mn, Ni, Mg, Ca and Pb) or $M(NO_3)_3$ (M = Al, Ga, In, Fe and Cr) or $M(ClO_4)_2$ (M = Fe) were dissolved in bis-tris buffer. Their UV-vis spectral changes were collected by adding corresponding amounts of Co^{2+} to **HBP** and blending them for 15 s.

For zinc ion, all fluorescence and UV-visible studies were conducted in DMF. A **HBP** stock was prepared in DMSO at 5 mM concentration and the concentration of **HBP** in all experiments was set as 5 μM. All metal ion stocks containing MNO_3 (M = Na and K) or $M(NO_3)_2$ (M = Zn, Co, Cd, Cu, Mn, Ni, Mg, Ca and Pb) or $M(NO_3)_3$ (M = Al, Ga, In, Fe and Cr) or $M(ClO_4)_2$ (M = Fe) were prepared in DMF. Their fluorescence and UV-vis spectral changes were collected by adding corresponding amounts of Zn^{2+} to **HBP** and blending them for 15 s.

Quantum yields

Quantum yields of **HBP** and **HBP**-Zn^{2+} were calculated with fluorescein (Φ = 0.79) as a reference fluorophore.[39] Quantum yield was given by using the following equation.[40]

$$\Phi_{F,S} = \Phi_{F,R} \times \frac{A_R \times F_S}{A_S \times F_R} \times \left(\frac{n_S}{n_R}\right)^2$$

where, Φ_F = fluorescence quantum yield; A = absorbance; F = integrated fluorescence emission; S = test sample; n = refractive index of the solvent; R = reference material.

Job plot measurements

To prepare **HBP** and Co^{2+} solutions at the same concentration of 50, 400 μL of a **HBP** stock (5 mM, DMSO) and 100 μL of Co^{2+} (2×10^{-2} M, bis-tris buffer) were diluted to 39.6 and 39.9 mL of buffer, respectively. Then, 2.7 – 0.3 mL of **HBP** solution and 0.3 – 2.7 mL of Co^{2+} solution were put into each UV-visible cell. Their total volume was set to be 3 mL. With blending for 10 s, UV-vis measurements with different concentration ratios were carried out.

To make **HBP** and Zn^{2+} solutions at the same concentration of 50 μM, 400 μL of a **HBP** stock (5×10^{-3} M, DMSO) and 100 μL of Zn^{2+} (2×10^{-2} M, DMF) were diluted to 39.6 and 39.9 mL of DMF, respectively. Then, 2.7 – 0.3 mL of **HBP** solution and 0.3 – 2.7 mL of Zn^{2+} solution were transferred to each fluorescent cell. Their total volume was set to be 3 mL. With blending for 10 s, fluorescent measurements with different concentration ratios were carried out.

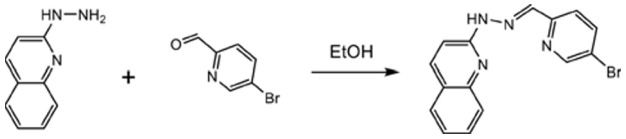

Scheme 1 Synthesis of **HBP**.

Computational studies

The Gaussian 16 program was used for the theoretical calculations to study detection mechanisms.[41] The optimized geometry and DFT calculations were performed on B3LYP/6-31G/LANL2DZ.[42-48] IEFPCM (integral equation formalism polarizable continuum model) was employed for considering the influence of the solvent.[49] Time-dependent DFT calculations were utilized to examine the electronic transition states of molecules. Among the 20 transition states, one calculation state, which best fits the experimental values, was chosen for the mechanism study.

Results and Discussion

The **HBP** was produced from the condensation reaction of 2-hydrazinylquinoline and 5-bromo-2-pyridinecarboxaldehyde (Scheme 1) and characterized by ESI-MS, ^{1}H NMR and ^{13}C NMR analysis (Fig. S1, Supporting Information).

*UV-vis studies of **HBP** to cobalt ion*

Colorimetric response of the **HBP** chemosensor toward a variety of metal ions was studied to investigate the sensing ability of the **HBP** in bis-tris buffer (Fig. 1). The **HBP** had a maximum absorption band at 365 nm. The addition of some metal ions like Cu^{2+}, Hg^{2+}, Ga^{3+}, Ag^+, and Fe^{2+} resulted in slight spectral variations with negligible color changes, whereas most metal ions induced no spectral variation at 512 nm. In contrast, the addition of Co^{2+} showed a marked spectral variation at 512 nm with a color change of colorless to pink. These outcomes meant that the **HBP** had a colorimetric sensing ability for Co^{2+}.

To explore the complexation mode of the **HBP** with Co^{2+}, Job plot analysis was carried out (Fig. S2). The maximum absorbance of 512 nm appeared at a mole fraction of 0.3, suggesting a 2 to 1 ratio of **HBP** to Co^{2+}. The result was verified by ESI-MS (Fig. S3). The peak of 709.67 (m/z) is indicative of [2·**HBP**-H$^+$ + Co^{2+}] (calcd; m/z 709.96).

UV-vis spectral variations were examined to study the sensing properties of **HBP** to Co^{2+} (Fig. 2). On the addition of Co^{2+} up to 0.65 equiv, the gradual increase of absorption bands at 250 and 512 nm and the gradual decrease of the absorption band at 360 nm appeared with the formation of a single isosbestic point at 268 nm. This indicated the production of a species between **HBP** with Co^{2+}. On the basis of the UV-vis spectra, the detection limit to Co^{2+} was found to be 10 nM by definition IUPAC ($C_{DL} = 3\sigma/k$) (R^2 = 0.9995) (Fig. 3).[50] The value is considerably lower than the WHO guideline (1.7 μM) and the lowest among sensors previously addressed for sensing both cobalt and zinc ions (Table S1).[51] The association constant was calculated to be 3×10^{11} M^{-2} with a suitable R^2 = 0.9974 by using Li equation (Fig. S4).[52]

To investigate the binding mode between **HBP** and Co^{2+}, FT-IR study was conducted (Fig. S5). In the case of **HBP**, the band at 3030 – 3200 cm^{-1} related to the –NH group was shown. Upon the binding with Co^{2+}, the band around 3200 cm^{-1}

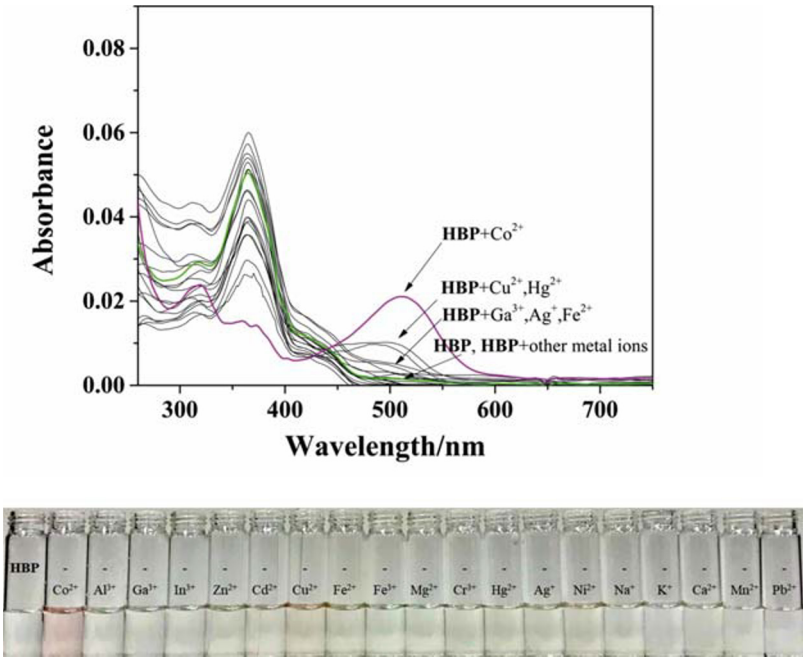

Fig. 1 Colorimetric response of **HBP** (2 μM, DMSO) to varied cations (0.65 equiv) in bis-tris buffer.

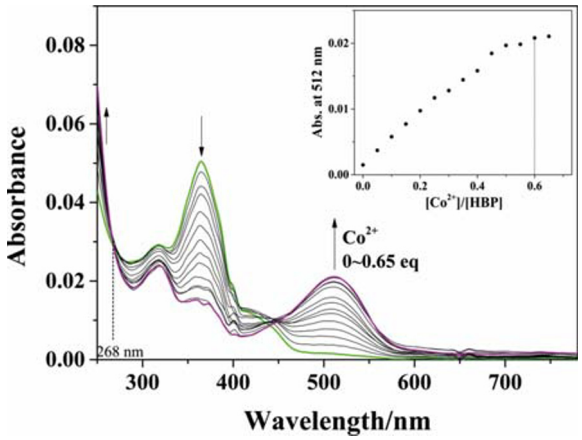

Fig. 2 UV-vis spectral variations of **HBP** upon the addition of Co^{2+} up to 0.65 equiv. Inset: plot of absorbance at 512 nm as a function of Co^{2+} equiv.

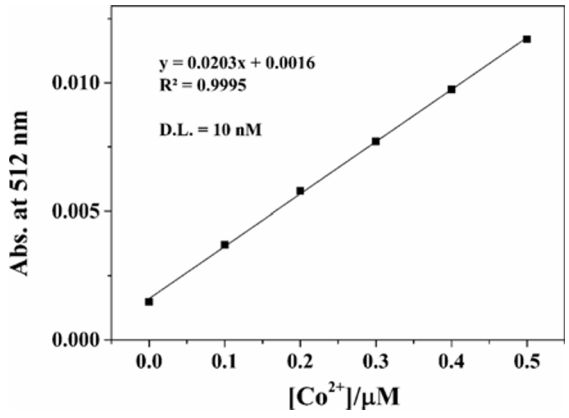

Fig. 3 Determination of detection limit of **HBP** toward Co^{2+}.

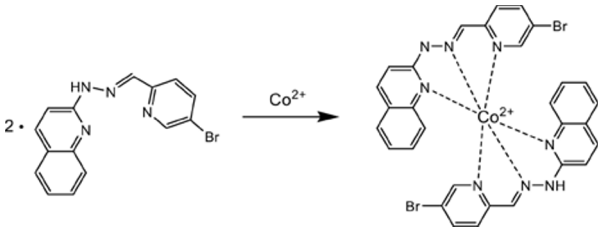

Scheme 2 Proposed binding of **HBP** to Co^{2+}.

disappeared and the band at 3030 cm^{-1} moved to 3050 cm^{-1}. It implied the deprotonation of one –NH group of two **HBP**. Meanwhile, the band of 1607 cm^{-1} related to the C=N bond showed a slight shift to 1599 cm^{-1}. These outcomes signified that the C=N and –NH groups of 2·**HBP** might be related to the binding to Co^{2+}. The binding mechanism of **HBP** and Co^{2+} was proposed, based on Job plot, FT-IR spectra and ESI-mass (Scheme 2).

To affirm the sensing capability of **HBP** to Co^{2+} when other metal ions exist, a competition test was performed (Fig. 4). In the existence of Ga^{3+}, Cr^{3+}, and Fe^{3+}, the sensing ability was disturbed by about 10 to 43%. However, most metal ions did not show any interference, pointing to the strong sensing ability of **HBP** to Co^{2+}. The pH test of **HBP** to Co^{2+} was carried out at a pH range of 6 to 9 (Fig. S6). On the addition of Co^{2+}, the immediate increase of absorbance at 512 nm and color change from colorless to pink were shown at a pH range of 6 to 9. It indicated that **HBP** could successfully detect Co^{2+} in the biological pH range (6.0 – 7.6).

*Fluorescence and UV-vis studies of **HBP** to zinc ion*

To investigate the fluorescent sensing ability of **HBP**, the fluorescent response of **HBP** to varied cations was studied in DMF (Fig. 5). **HBP** had no fluorescence emission at 560 nm and the addition of other metal ions except Zn^{2+}, caused no or

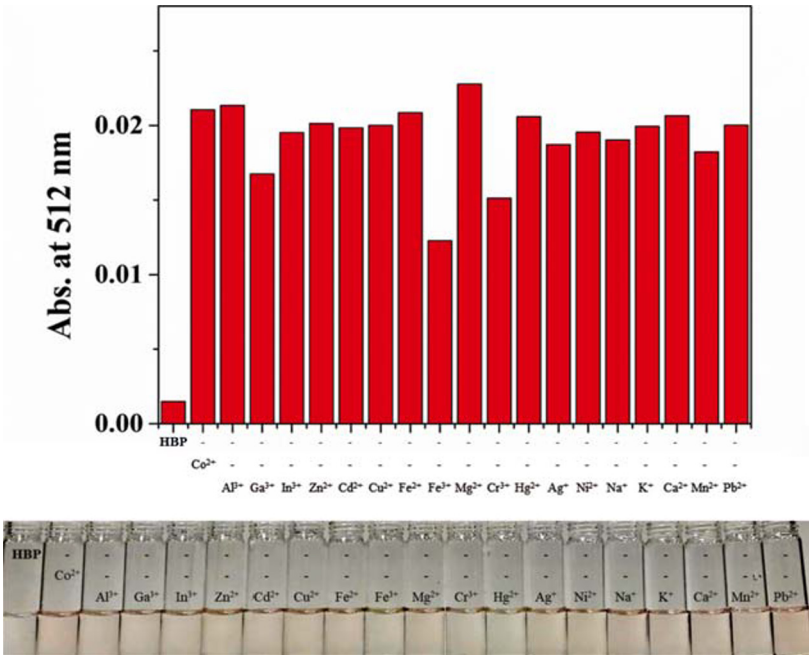

Fig. 4 Competitions test of **HBP** to Co^{2+} with other cations.

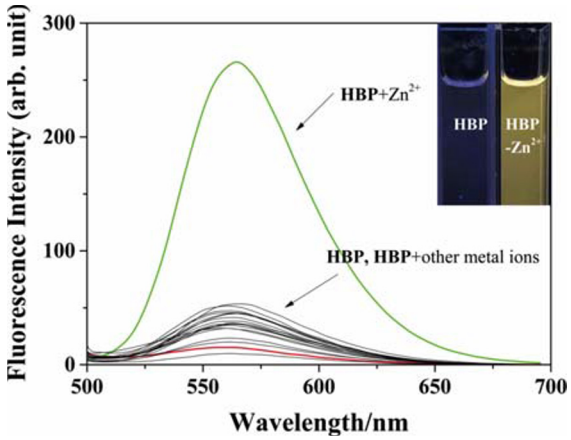

Fig. 5 Fluorescent response of **HBP** (5 μM, DMSO) to varied cations (0.54 equiv, DMF) in DMF. Inset: fluorescent photograph of **HBP** and **HBP**-Zn^{2+}.

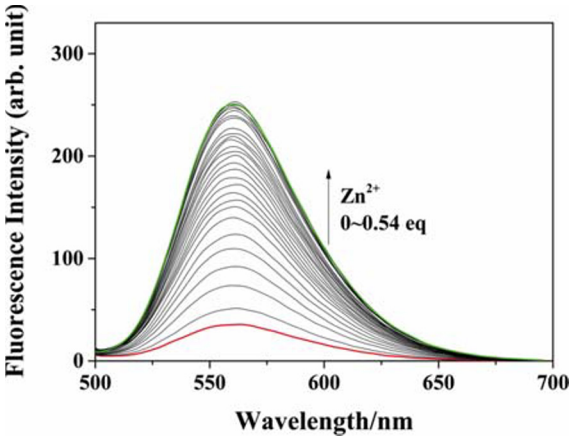

Fig. 6 Fluorescence titrations of **HBP** with different equivalents of Zn^{2+} up to 0.54 equiv.

negligible spectral variations at 560 nm. In contrast, only Zn^{2+} showed an obvious fluorescence increase at 560 nm (λ_{ex} = 480 nm) with a yellow fluorescence color. It indicated that **HBP** had a fluorescent sensing response to Zn^{2+}.

To investigate the complexation ratio of **HBP** and Zn^{2+}, Job plot analysis was carried out (Fig. S7). The maximum fluorescence intensity at 560 nm appeared at a mole fraction of 0.3, which implied a 2 to 1 ratio of **HBP** to Zn^{2+}. As shown in Fig. S8, it was further verified by ESI-MS. The peak of 715.25 (*m*/*z*) is indicative of [2·**HBP**-H^+ + Zn^{2+}] (calcd; *m*/*z* 714.95).

Fluorescent and UV-visible variations were studied to explore the sensing properties of **HBP** to Zn^{2+}. Upon the addition of Zn^{2+} up to 0.54 equiv (Fig. 6), the gradual enhancement of fluorescent intensity at 560 nm was observed with an obvious change of quantum yield (Φ) of 0.017 to 0.120. Under the same conditions, the addition of Zn^{2+} up to 0.5 equiv induced the gradual increase of absorbance at 300 and 515 nm and the decrease of absorbance at 355 nm with two marked isosbestic points at 315 and 394 nm (Fig. S9). The outcome meant the formation of a species of **HBP** with Zn^{2+}.

Based on the fluorescent spectra, the detection limit for zinc ion turned out to be 18 nM by definition IUPAC ($C_{DL} = 3\sigma/k$) (R^2 = 0.9977) (Fig. S10).[50] The value is significantly lower than the WHO guideline (76 μM) and can be expressed down to the nanomolar unit.[51] The association constant was calculated to be 2×10^{11} M^{-2} with an adequate R^2 = 0.9959 with the determination of Li's equation (Fig. S11).[52]

To study the binding mode between **HBP** and Zn^{2+}, FT-IR spectra were obtained (Fig. S12). Similar to those of **HBP**-Co^{2+}, the band around 3030 – 3200 cm^{-1} related to the –NH groups were broadened and the band of 3030 cm^{-1} moved to 3050 cm^{-1}. It implied the deprotonation of one –NH group of two **HBP**. Meanwhile, the band at 1607 cm^{-1} related to the C=N

bond moved slightly to 1604 cm^{-1}. These results suggested that the C=N and –NH groups might be related to the binding to zinc ion. Binding mechanism of **HBP** and Zn^{2+} was proposed, based on Job plot, FT-IR spectra and ESI-MS (Scheme 3).

A competition test was conducted to check the sensing ability of **HBP** toward Zn^{2+} (Fig. S13). Most metal ions showed no inhibition effect, whereas some metal ions like Hg^{2+}, Cu^{2+}, Cd^{2+}, and Ni^{2+} caused interference of 30 to 50%, while Fe^{2+} and Co^{2+} completely interfered due to their paramagnetic properties.

Computational studies to Zn^{2+}

The optimized structures of **HBP** and **HBP**-Zn^{2+} were obtained based on experimental results, such as Job plot, ESI-mass, and FT-IR (Fig. 7). **HBP** and **HBP**-Zn^{2+} exhibited planar and crossed-planar structures with dihedral angles of 0.000° and 1.968° (1N, 2N, 3C, 4N), respectively.

The possible transition states and molecular orbitals were explored using time-dependent DFT calculations. For **HBP**, the main absorption at 373.27 nm stemmed from HOMO → LUMO transition, which presented π–π* transition characteristic (Figs. S14 and S15). The red-shifted major transition of **HBP**-Zn^{2+} derived from HOMO → LUMO + 1 transition, which also displayed π–π* transition character (Figs. S15 and S16). Considering the similarity in transition properties and structures of **HBP** and **HBP**-Zn^{2+}, the fluorescent turn-on process may be a CHEF (chelation enhanced fluorescence) effect. As zinc chelated, non-radiative transitions such as rotation and vibration would be suppressed and switched into radiative transitions. Based on these results, we proposed a feasible zinc detection mechanism of **HBP** (Scheme 3).

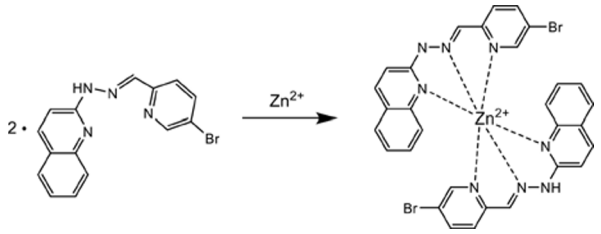

Scheme 3 Proposed binding of **HBP** to Zn^{2+}.

Conclusions

A new heterocyclic-based bifunctional sensor, **HBP**, was developed. The **HBP** had successful responses to cobalt in bis-tris buffer and zinc ions in DMF, showing the outstanding color and fluorescence change, respectively. On the other hand, the **HBP** chemosensor can detect only Co^{2+} in aqueous solution. The significantly low detection limits were calculated as 10 nM for cobalt ion and 18 nM for zinc ion. Especially, the detection limit for cobalt was the lowest among the sensors formerly addressed for detecting both cobalt and zinc ions. In particular, **HBP** is the first chemosensor that offers detection limits down to the nanomolar unit for both cobalt and zinc ions. The binding mechanisms to cobalt and zinc ions were demonstrated with UV-vis and fluorescent spectral variations, Job plot, FT-IR, ESI-MS and calculations.

Acknowledgements

The authors acknowledge their appreciation to the National Research Foundation of Korea (NRF-2018R1A2B6001686).

Supporting Information

UV-visible spectra, FT-IR and ESI-MS spectra, energy-optimized structures, electronic transition energies and molecular orbital spectra are provided.

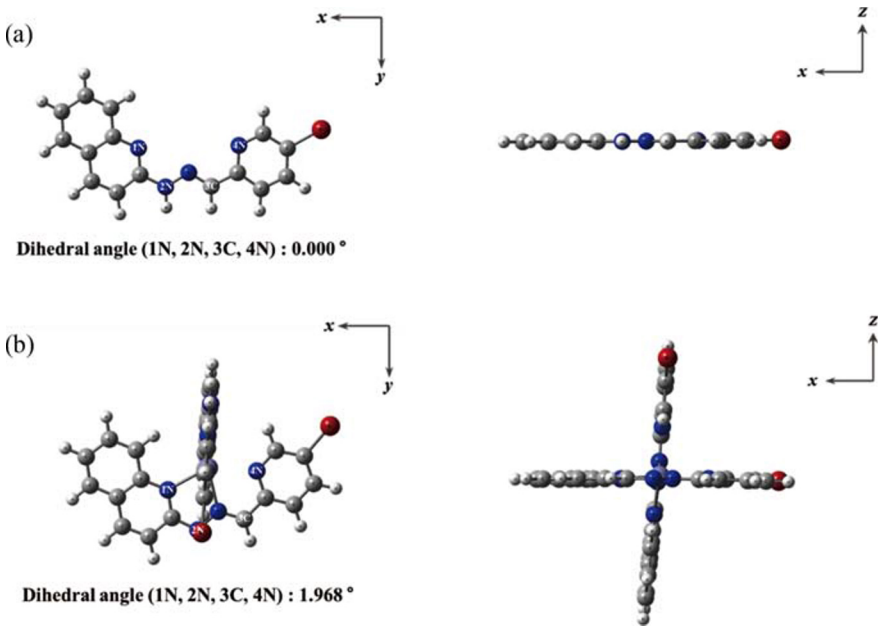

Fig. 7 Energy-optimized forms of (a) **HBP** and (b) **HBP**-Zn^{2+}.

References

1. V. Raju, R. Selva Kumar, S. K. Ashok Kumar, Y. Tharakeswar, and S. K. Sahoo, *Inorg. Chem. Commun.*, **2019**, *101*, 74.
2. M. Yang, L. Ma, J. Li, and L. Kang, *RSC Adv.*, **2019**, *9*, 16812.
3. W. Sik Na, P. Raj, N. Singh, and D. O. Jang, *Tetrahedron Lett.*, **2019**, *60*, 151075.
4. D. Maity, D. Karthigeyan, T. K. Kundu, and T. Govindaraju, *Sens. Actuators, B*, **2013**, *176*, 831.
5. W. Du, R.-J. Liu, J. Fang, H. Gao, Y.-W. Wang, and Y. Peng, *Tetrahedron*, **2019**, *75*, 130477.
6. T. B. Wei, B. R. Yong, L. R. Dang, Y. M. Zhang, H. Yao, and Q. Lin, *Dyes Pigm.*, **2019**, *171*, 107707.
7. Z. Gu, H. Cheng, X. Shen, T. He, K. Jiang, H. Qiu, Q. Zhang, and S. Yin, *Spectrochim. Acta, Part A*, **2018**, *203*, 315.
8. S. C. Lee and C. Kim, *Anal. Sci.*, **2019**, *35*, 1189.
9. Y. M. Kho and E. J. Shin, *Molecules*, **2017**, *22*, 1569.
10. K. Jiang, S. Chen, S. Luo, C. Pang, X. Wu, and Z. Wang, *Dyes Pigm.*, **2019**, *167*, 164.
11. J. Li, Y. Chen, T. Chen, J. Qiang, Z. Zhang, T. Wei, W. Zhang, F. Wang, and X. Chen, *Sens. Actuators, B*, **2018**, *268*, 446.
12. H. J. Jang, J. B. Chae, J. M. Jung, H. So, and C. Kim, *Bull. Korean Chem. Soc.*, **2019**, *40*, 650.
13. Y. Li, Z. Gu, T. He, X. Yuan, Y. Zhang, Z. Xu, H. Qiu, Q. Zhang, and S. Yin, *Dyes Pigm.*, **2020**, *173*, 107969.
14. N. Narayanaswamy, D. Maity, and T. Govindaraju, *Supramol. Chem.*, **2011**, *23*, 703.
15. V. Venkatesan, S. Kumar R, S. K. A. Kumar, and S. K. Sahoo, *Inorg. Chem. Commun.*, **2019**, *102*, 171.
16. G. Zhao, B. Guo, G. Wei, S. Guang, Z. Gu, and H. Xu, *Dyes Pigm.*, **2019**, *170*, 107614.
17. D. Maity and T. Govindaraju, *Inorg. Chem.*, **2011**, *50*, 11282.
18. S. Patil, U. Fegade, S. K. Sahoo, A. Singh, J. Marek, N. Singh, R. Bendre, and A. Kuwar, *ChemPhysChem*, **2014**, *15*, 2230.
19. X. Wang, W. Zheng, H. Lin, G. Liu, Y. Chen, and J. Fang, *Tetrahedron Lett.*, **2009**, *50*, 1536.
20. M. An, B. Y. Kim, H. Seo, A. Helal, and H. S. Kim, *Spectrochim. Acta, Part A*, **2016**, *169*, 87.
21. K. Ponnuvel, M. Kumar, and V. Padmini, *Sens. Actuators B*, **2016**, *227*, 242.
22. M. Sohrabi, M. Amirnasr, H. Farrokhpour, and S. Meghdadi, *Sens. Actuators, B*, **2017**, *250*, 647.
23. B. Das, A. Jana, A. Das Mahapatra, D. Chattopadhyay, A. Dhara, S. Mabhai, and S. Dey, *Spectrochim. Acta, Part A*, **2019**, *212*, 222.
24. M. Hagimori, M. Taniura, N. Mizuyama, Y. Karimine, S. Kawakami, H. Saji, and T. Mukai, *Sensors*, **2019**, *19*, 2049.
25. G. J. Park, J. J. Lee, G. R. You, L. Nguyen, I. Noh, and C. Kim, *Sens. Actuators, B*, **2016**, *223*, 509.
26. S. Y. Lee, S. Y. Kim, J. A. Kim, and C. Kim, *J. Lumin.*, **2016**, *179*, 602.
27. L. L. Gao, S. P. Li, Y. Wang, W. N. Wu, X. L. Zhao, H. J. Li, and Z. H. Xu, *Spectrochim. Acta, Part A*, **2020**, *230*, 118025.
28. M. Sohrabi, M. Amirnasr, S. Meghdadi, M. Lutz, M. Bikhof Torbati, and H. Farrokhpour, *New J. Chem.*, **2018**, *42*, 12595.
29. N. N. Li, C. F. Bi, X. Zhang, C. G. Xu, C. Bin Fan, W. S. Gao, Z. A. Zong, S. S. Zuo, C. F. Niu, and Y. H. Fan, *J. Photochem. Photobiol. A*, **2020**, *390*, 112299.
30. Y. Wang, D. Qiu, M. Li, Y. Liu, H. Chen, and H. Li, *Spectrochim. Acta, Part A*, **2017**, *185*, 256.
31. Y. Q. Gu, W. Y. Shen, Y. Zhou, S. F. Chen, Y. Mi, B. F. Long, D. J. Young, and F. L. Hu, *Spectrochim. Acta, Part A*, **2019**, *209*, 141.
32. Z. Long, M. Liu, R. Jiang, Q. Wan, L. Mao, Y. Wan, F. Deng, X. Zhang, and Y. Wei, *Chem. Eng. J.*, **2017**, *308*, 527.
33. Y. Y. Zhu, Q. Sun, J. W. Shi, H. Y. Xia, J. L. Wang, H. Y. Chen, H. F. He, L. Shen, F. Zhao, and J. Zhong, *J. Photochem. Photobiol. A*, **2020**, *389*, 112244.
34. A. Pandith, N. Uddin, C. H. Choi, and H.-S. Kim, *Sens. Actuators, B*, **2017**, *247*, 840.
35. D. Yun, J. B. Chae, H. So, H. Lee, K. T. Kim, and C. Kim, *New J. Chem.*, **2019**, *44*, 442.
36. A. Kim and C. Kim, *New J. Chem.*, **2019**, *43*, 7320.
37. S. N. Karuk Elmas, Z. E. Dincer, A. S. Erturk, A. Bostanci, A. Karagoz, M. Koca, G. Sadi, and I. Yilmaz, *Spectrochim. Acta, Part A*, **2020**, *224*, 117402.
38. J. T. Pan, F. Zhu, L. Kong, L. M. Yang, X. T. Tao, Y. P. Tian, H. B. Lu, and J. X. Yang, *Chem. Pap.*, **2015**, *69*, 527.
39. D. Magde, R. Wong, and P. G. Seybold, *Photochem. Photobiol.*, **2004**, *75*, 327.
40. C. Kim and J. B. Chae, *J. Fluoresc.*, **2018**, *28*, 1363.
41. Gaussian 16, Gaussian.com.
42. A. D. Becke, *J. Chem. Phys.*, **1993**, *98*, 5648.
43. C. Lee, W. Yang, and R. G. Parr, *Phys. Rev. B*, **1988**, *37*, 785.
44. P. C. Hariharan and J. A. Pople, *Theor. Chim. Acta*, **1973**, *28*, 213.
45. M. M. Francl, W. J. Pietro, W. J. Hehre, J. S. Binkley, M. S. Gordon, D. J. DeFrees, and J. A. Pople, *J. Chem. Phys.*, **1982**, *77*, 3654.
46. P. J. Hay and W. R. Wadt, *J. Chem. Phys.*, **1985**, *82*, 270.
47. W. R. Wadt and P. J. Hay, *J. Chem. Phys.*, **1985**, *82*, 284.
48. P. J. Hay and W. R. Wadt, *J. Chem. Phys.*, **1985**, *82*, 299.
49. A. Klamt, C. Moya, and J. Palomar, *J. Chem. Theory Comput.*, **2015**, *11*, 4220.
50. S. Goswami, K. Aich, S. Das, C. Das Mukhopadhyay, D. Sarkar, and T. K. Mondal, *Dalton. Trans.*, **2015**, *44*, 5763.
51. World Health Organization, "WHO Guidelines for Drinking Water Quality", 2nd ed., **1998**, Vol. 2, 3 – 81.
52. N. Shao, Y. Zhang, S. M. Cheung, R. H. Yang, W. H. Chan, T. Mo, K. A. Li, and F. Liu, *Anal. Chem.*, **2005**, *77*, 7294.